High-precision inverse potentials for neutron-proton scattering using piece-wise smooth Morse functions*

Ayushi Awasthi[1†] Arushi Sharma[1‡] Ishwar Kant[1§] O. S. K. S. Sastri[1¶]

[1]Department of Physics and Astronomical Science, Central University of Himachal Pradesh, Dharmshala, 176215, India

Abstract: The aim of this study is to construct inverse potentials for various ℓ-channels of neutron-proton scattering using a piece-wise smooth Morse function as a reference. The phase equations for single-channel states and the coupled equations of multi-channel scattering are solved numerically using the 5th order Runge-kutta method. We employ a piece-wise smooth reference potential comprising three Morse functions as the initial input. Leveraging a machine learning-based genetic algorithm, we optimize the model parameters to minimize the mean-squared error between simulated and anticipated phase shifts. Our approach yields inverse potentials for both single and multi-channel scattering, achieving convergence to a mean-squared error $\leq 10^{-3}$. The resulting scattering lengths "a_0" and effective ranges "r" for $^3S_1$ and $^1S_0$ states, expressed as [a_0, r], are found to be [5.445(5.424), 1.770(1.760)] fm and [–23.741(–23.749), 2.63(2.81)] fm, respectively; these values are in excellent agreement with experimental ones. Furthermore, the calculated total scattering cross-sections are highly consistent with their experimental counterparts, having a percentage error of less than 1%. This computational approach can be easily extended to obtain interaction potentials for charged particle scattering.

Keywords: inverse potentials, neutron-proton scattering, piece-wise smooth Morse function, phase function method, reference potential approach, genetic algorithm

DOI: 10.1088/1674-1137/ad5d63

I. INTRODUCTION

Current high-precision nucleon-nucleon potentials, available for scattering data up to the pion-threshold of 350 MeV, are provided by various groups; these include the Argonne v_{18} [1], Bonn [2], Reid [3], Nijmegen [4], and Paris [5] potentials. These potentials are modeled such that the NN interaction comprises one pion exchange potential for long inter-nuclear distances of $r \geq 2$ fm. The main differences between these high precision potentials stem from the way the nucleon-nucleon interaction is modeled for intermediate/medium (1.0 fm < r < 2 fm) and short-ranges (r < 1.0 fm) [6]. This modeling is performed using a central potential along with an interplay of orbital, tensor, spin-orbit, and quadratic spin-orbit terms. The approach involves simultaneously solving for the wave-functions based on the model potential and optimizing approximately 40−50 parameters for obtaining the phase shifts for all ℓ-channels for nucleon-nucleon scattering, from which the total cross sections are predicted to match the experimental ones [7]. An alternative methodology is to construct the inverse potentials utilizing the phase function method or variable phase approximation [8–10], which has the advantage of obtaining phase shifts by directly utilizing the potential, without the wave-function. Here, the second-order time-independent Schrödinger equation is transformed into a set of independent first-order non-linear Ricatti equations for each ℓ channel. Thus, one can determine the potentials corresponding to phase shifts for individual channels. This methodology is equivalent to constructing the model potential directly from the available scattering phase shifts data, which is the basic premise of the machine learning paradigm [11, 12].

Ideally, to obtain a complete inverse scattering solution, N discrete bound state energies $E_n < 0$ (n = 1, 2, …, N) and all possible scattering phase shifts for energies $E >$ 0, up to ∞, are required [13]. However, the available experimental data are limited to very few projectile energy values. Hence neural network-based machine learning models are not suitable, and we propose to utilize meta-

Received 10 May 2024; Accepted 1 July 2024; Published online 2 July 2024

* Support provided by Department of Science and Technology (DST), Government of India vide Grant No. DST/INSPIRE Fellowship/2020/IF200538

† E-mail: awasthiayushi1998@gmail.com

‡ E-mail: 97arushi19@gmail.com

§ E-mail: ishwrknt@gmail.com

¶ E-mail: sastri.osks@hpcu.ac.in

heuristic genetic algorithms (GAs) for constructing model potentials by optimizing the parameters of the chosen reference function to guide the process. The phase equation arising from the phase function method is incorporated in the optimization procedure, and the bounds for various parameters are chosen to obtain physically relevant potentials. This is the essence of physics-informed machine learning [14], representing a progressive approach for solving complex problems in computational sciences.

Selg [13, 15] proposed the Morse function as an ideal choice for the reference function to construct inverse potentials due to its various advantages. It provides the analytical solution of the time-independent Schrödinger equation for ℓ=0. Moreover, the Morse function can represent all characteristics of nucleon-nucleon interactions such as repulsion at short inter-nuclear distances, attraction at intermediate distances, and quick falling of the tail at large distances. Previously, inverse potentials for all ℓ channels of *np* scattering were constructed using the phase function method by taking the Morse function as a zeroth reference [16]. The Deuteron structure and form factors were determined from the analytical ground state wavefunction [17]. These were achieved by implementing an innovative algorithm based on a variation of the variational Monte-Carlo technique [18], which was cast as an optimization routine. It was an equivalent alternative to the least squares minimization approach.

One can observe the complex nature of nucleon-nucleon interactions, as envisaged by various researchers who have obtained realistic precision potentials, comprising considerably different characteristics for the three regions. Therefore, considering a single Morse function limits the space of curves available for convergence to the required inverse potentials.

In principle, one can construct inverse potentials by solving the phase equation, for a potential $V(r)$, iteratively within the machine learning-based optimization algorithm. The idea is to start with an initial potential array $V[i] = V[r_i]$. Here, r_i is an array of uniformly sampled values in an interval of $[0, r_f]$, where r_f is the distance beyond which the interaction is assumed to be negligible. One can initialize the potential value V_i at various points r_i randomly, just as one would initialize the wavefunction values ψ_i at various r_i in the variational Monte Carlo approach for determining the ground state energy of a physical system [19]. However, an important difference between solving the time-independent Schrödinger equation and phase equation is as follows. While the wavefunction and its second derivative are evaluated in every iteration to determine the energy in the variational Monte Carlo approach using the Hamiltonian of the time-independent Schrödinger equation, the potential appears in the phase equation only as a multiplicative function. Therefore, while solving the time-independent Schrödinger equation ensures the evolving wavefunction solution to remain smooth, the resulting potential from the phase equation does not. Thus, we need to rely on certain smooth mathematical functions as a reference for initializing the algorithm. The variation of parameters of the reference function would generate a large number of curves in the sample space. The nature of the curves depends on the bounds chosen for each of the individual parameters of the reference potential. The inverse potential that best describes the expected phase shifts is obtained by optimizing the parameters of the reference function by minimizing a cost function such as the mean squared error (MSE). The methodology of constructing inverse potentials by solving the phase equation utilizing the reference function is called the reference potential approach [13]. Generally, a multi-component potential composed of a smoothly joined Morse type, *i.e.*, piece-wise smooth, Morse function is used in this approach [12]. A three-component Morse potential was successfully utilized by Selg [20] for obtaining the molecular interaction potentials.

In this study, we consider the same reference to construct the inverse potentials for various ℓ-channels of np scattering for energies up to 350 MeV. Thus, we numerically solve the phase equation for single-channel scattering for various ℓ-channels and successfully implement the "Stapp-Parametrization" to incorporate mixing parameters, for many-channel scattering [10]. The latter technique involves solving three coupled non-linear differential phase equations. Our computational approach involves solving these single and coupled differential equations iteratively within a GA based optimization routine [21] to obtain the best parameters for the piece-wise smooth Morse curve, consisting of three functions, to minimize the MSE as the cost function.

II. METHODOLOGY

In this section, we explain the necessary models used in the paper. We demonstrate the non-linear relationship between observables and the scattering potential, focusing on nuclear scattering experiments. Subsequently, we elaborate on the Reference Potential Approach (RPA), where we employ a piece-wise Morse function as a reference to solve non-linear equations. Subsequently, we discuss the machine learning-based optimization algorithm used to optimize model parameters, yielding high-precision neutron-proton interaction potentials.

A. Variable phase approximation

To represent the forward problem of nuclear scattering, one must solve the 3*D* time-independent Schrödinger equation [22]. This is a linear, second-order partial differential equation that describes the evolution of the $\psi(r)$ wave functions under a scattering potential $V(r)$. The

problem can be simplified into solving the radial Schrödinger equation, which is defined as follows:

$$\frac{\mathrm{d}^2u_\ell(k,r)}{\mathrm{d}r^2}+\left(k^2-\frac{\ell(\ell+1)}{r^2}\right)u_\ell(k,r)=U(r)u_\ell(k,r), \tag{1}$$

where $k=\sqrt{\frac{2\mu E_{\rm cm}}{\hbar^2}}$, $U(r)=\frac{2\mu V(r)}{\hbar^2}$, and μ is the reduced mass of the system.

$E_{\rm cm}$ is related to $E_{\ell ab}$ as $E_{\rm cm}=\frac{m_T}{m_T+m_P}E_{\ell ab}$. Here, m_T and m_P are the masses of the target and projectile, respectively. In scattering experiments, we concentrate on the asymptotic nature of wave functions, which are represented by the sum of an incoming plane wave $\mathrm{e}^{\mathrm{i}kr}$ and an outgoing spherical wave, weighted by the scattering amplitude $f(k,\theta)$ and related to the differential cross section as [22]

$$\frac{\mathrm{d}\sigma}{\mathrm{d}\omega}=|f(k,\theta)|^2, \tag{2}$$

The scattering amplitude and phase shifts can be expressed using a partial wave expansion, resulting in the following form [22]:

$$f(k,\theta)=\frac{1}{2\mathrm{i}k}\sum(2\ell+1)(\mathrm{e}^{2\mathrm{i}\delta_\ell}-1)P_\ell(\cos\theta), \tag{3}$$

where P_ℓ is the ℓ^{th} order Legendre polynomial, and $\delta_{l\ell}$ is the phase shift of the ℓ^{th} partial wave. In scattering experiments, differential and total cross sections are measured, and phase shifts are obtained by fitting different partial waves. Therefore, solving the Schrödinger equation by fitting the expected asymptotic wavefunction and obtaining the phase shifts is the forward problem.

However, the variable phase approximation or phase function method addresses the inverse problem, where the linear homogeneous equation of the second order can be reduced to the first order Ricatti equation. This approach suggests that a function fulfilling the Riccati equation, known as a phase function, represents the phase shift of the wave function at each point during scattering by a potential that is truncated at that point, in contrast to the case of unhindered motion [10, 23]. Now, we discuss an exact equation for phase functions, which can aid actual numerical computations. The most important cases associated with potential scattering are considered.

1. *Single channel scattering*

Consider elastic scattering by a central potential or an arbitrary potential that does not result in mixing of partial waves with different orbital angular moments (*i.e.*, one-channel reaction). Hence, the second order TISE is transformed into Ricatti type equation [9, 10, 24], which is given by

$$\frac{\mathrm{d}\delta_\ell(k,r)}{\mathrm{d}r}=-\frac{U(r)}{k}\left[\cos(\delta_\ell(k,r))\hat{j}_\ell(kr)-\sin(\delta_\ell(k,r))\hat{\eta}_\ell(kr)\right]^2, \tag{4}$$

where $U(r)=\frac{2\mu V(r)}{\hbar^2}$.

The initial point for the phase equation is $\delta_\ell(r=0)=0$, indicating zero phase shift, where the potential has not yet affected the incoming wave. The ultimate phase shift measured, $\delta_\ell(r\to\infty)$, represents the accumulated phase shift as the distance approaches infinity. This equation finds utility in atomic and nuclear physics for determining the scattering phase shift corresponding to a specific potential.

The Riccati Hankel function of the first kind is related to $\hat{j}_\ell(kr)$ and $\hat{\eta}_\ell(kr)$ as $\hat{h}_\ell(r)=-\hat{\eta}_\ell(r)+\mathrm{i}\,\hat{j}_\ell(r)$. For $\ell=0$, the Ricatti-Bessel and Riccati-Neumann functions $\hat{j}_0$ and $\hat{\eta}_0$ get simplified as $\sin(kr)$ and $-\cos(kr)$. Therefore, the phase equation for ℓ=0 is [18]

$$\delta_0'(k,r)=-\frac{U(r)}{k}\sin^2[kr+\delta_0(r)], \tag{5}$$

For higher partial waves, the Ricatti-Bessel and Riccati-Neumann functions used in the PFM can be easily obtained using the following recurrence formulas [16]:

$$\hat{j}_{\ell+1}(kr)=\frac{2\ell+1}{kr}\hat{j}_\ell(kr)-\hat{j}_{\ell-1}(kr), \tag{6}$$

$$\hat{\eta}_{\ell+1}(kr)=\frac{2\ell+1}{kr}\hat{\eta}_\ell(kr)-\hat{\eta}_{\ell-1}(kr), \tag{7}$$

The phase function equation for ℓ=1 and 2 takes following form:

$$\delta_1'(k,r)=-\frac{U(r)}{k}\left[\frac{\sin(\delta_1+(kr))-(kr)\cos(\delta_1+(kr))}{(kr)}\right]^2, \tag{8}$$

$$\delta_2'(k,r)=-\frac{U(r)}{k}\left[-\sin(\delta_2+(kr))-\frac{3\cos(\delta_2+(kr))}{(kr)}+\frac{3\sin(\delta_2+(kr))}{(kr)^2}\right]^2, \tag{9}$$

Similarly, the phase function equations can be obtained for higher partial waves using Eqs. (6) and (7).

Equation (4) is a non-linear equation and can be

solved numerically using the 5th order Runge-Kutta (RK-5) method with the initial condition $\delta_\ell(k,0)=0$.

2. *Multi-channel scattering*

The phase function method can be expanded to encompass scenarios involving a non-central tensor interaction and multi-channel inelastic scattering. A notable instance is the elastic scattering interaction between two particles with spin 1/2, such as nucleons, wherein the tensor interaction is considered. In the triplet spin state, the tensor forces $T_j(r)$ intermix the partial waves, leading to different orbital angular momenta $\ell = J \mp 1$ for a given total angular momentum J of the system. Consequently, the equations governing the radial wave functions $u_J(r)$ and $w_J(r)$ are interrelated as [10, 22]

$$\frac{\mathrm{d}^2u_J(k,r)}{\mathrm{d}r^2}+\left(k^2-\frac{J(J-1)}{r^2}-V_{J,J-1}\right)u_J(k,r)-T_jw_J(k,r)=0,$$

$$\frac{\mathrm{d}^2w_J(k,r)}{\mathrm{d}r^2}+\left(k^2-\frac{(J+2)(J+1)}{r^2}-V_{J,J+1}\right)\times w_J(k,r)-T_ju_J(k,r)=0, \tag{10}$$

The coupling of Eq. (10) complicates the calculation of scattering phase shifts, which involves two phase shifts and a mixing component. For small r, one of the system's linearly independent solutions is significantly larger than the other. It is challenging to "extract" the gradually growing solution from the background of the initial solution. The PFM allows us to obtain a straightforward set of first-order linear equations for three functions and eliminate this drawback. It is widely recognized that a tensor potential permits a distinct parametrization of the scattering matrix. Various representations of these parameters within the PFM equations have been developed in studies by Kynch [25], Babikov [26], and Cox and Perlmutter [27].

In this study, we focus solely on the equations for the functions $\delta_{J,J-1}(r)$, $\delta_{J,J+1}(r)$, and $\epsilon_J(r)$, which are associated with "Stapp parametrization," widely employed in nuclear physics [26, 28]. In neutron-proton scattering, multiple-channel scattering occurs. For the state with angular momentum $J=1$, mixing of the $^3S_1$ and $^3D_1$ states occurs with a mixing parameter ϵ_1. For $J=2$, mixing of the $^3P_2$ and $^3F_2$ states occurs with a mixing parameter ϵ_2. For $J=3$, mixing of the $^3D_3$ and $^3G_3$ states occurs with a mixing parameter ϵ_3. For $J=4$, mixing of the $^3F_4$ and $^3H_4$ states occurs with a mixing parameter ϵ_4.

Therefore, the equations for Stapp parameterization can be written for a particular J as

$$\frac{\mathrm{d}\delta_{J,J-1}}{\mathrm{d}r}=\frac{-1}{k\cos 2\epsilon_J}\Big[V_{J,J-1}\left(\cos^4\epsilon_JP^2_{J,J-1}-\sin^4\epsilon_JQ^2_{J,J-1}\right)-V_{J,J+1}\sin^2\epsilon_J\cos^2\epsilon_J\left(P^2_{J,J+1}-Q^2_{J,J+1}\right)-2T_J\sin\epsilon_J\cos\epsilon_J\left(\cos^2\epsilon_JP_{J,J-1}Q_{J,J+1}-\sin^2e_JP_{J,J+1}Q_{J,J-1}\right)\Big], \tag{11}$$

$$\frac{\mathrm{d}\delta_{J,J+1}}{\mathrm{d}r}=\frac{-1}{k\cos 2\epsilon_J}\Big[V_{J,J+1}\left(\cos^4\epsilon_JP^2_{J,J+1}-\sin^4\epsilon_JQ^2_{J,J+1}\right)-V_{J,J-1}\sin^2\epsilon_J\cos^2\epsilon_J\left(P^2_{J,J-1}-Q^2_{J,J-1}\right)-2T_J\sin\epsilon_J\cos\epsilon_J\left(\cos^2\epsilon_JP_{J,J+1}Q_{J,J-1}-\sin^2\epsilon_JP_{J,J-1}Q_{J,J+1}\right)\Big], \tag{12}$$

$$\frac{\mathrm{d}\epsilon_J}{\mathrm{d}r}=\frac{-1}{k}\Big[T_J\left(\cos^2\epsilon_JP_{J,J-1}P_{J,J+1}+\sin^2\epsilon_JQ_{J,J-1}Q_{J,J+1}\right)-V_{J,J-1}\sin\epsilon_J\cos\epsilon_JP_{J,J-1}Q_{J,J-1}-V_{J,J+1}\sin\epsilon_J\cos\epsilon_JP_{J,J+1}Q_{J,J+1}\Big], \tag{13}$$

where $P_{J,\ell}(r)$ and $Q_{J,\ell}(r)$ can be defined as

$$P_{J,\ell}(r)=\cos(\delta_{J,\ell}(r))\hat{j}_\ell(kr)-\sin(\delta_{J,\ell}(r))\hat{\eta}_\ell(kr),$$
$$Q_{J,\ell}(r)=\sin(\delta_{J,\ell}(r))\hat{j}_\ell(kr)+\cos(\delta_{J,\ell}(r))\hat{\eta}_\ell(kr),$$

Equations (11)−(13) are three non-linear coupled first order equations, which can be solved using RK-5 with initial conditions $\delta_{J,J-1}(0)=0$, $\delta_{J,J+1}(0)=0$, and $e_J(0)=0$.

Thus, in this study, we investigated single channel and multi- channel scattering using the phase function method by employing the reference potential approach.

B. Reference potential approach

Selg [13, 15] recommends the reference potential approach for solving 1D quantum systems wherein a single Morse function [13] or a combination of smoothly joined Morse functions of the form

$$U_i^{\mathrm{RPA}}(r)=V_i+D_j[\mathrm{e}^{-2\alpha_i(r-r_i)}-2\mathrm{e}^{-\alpha_i(r-r_i)}]\quad i=0,1,2\ldots, \tag{14}$$

can be chosen as the starting point to solve the time-independent Schrödinger equation for its energy eigenvalues and scattering phase shifts, as well as the Jost function for the inverse potential [12].

Here, $D_i$represents the potential depths at equilibrium distances r_i, and α_i represents the shape parameter of

Morse functions. V_i represents the constants added to the total potential, whose importance is clarified later. These functions are smoothly joined at various boundary points x_{i+1}.

The number of distinct Morse-type components that may be added is almost unlimited. Naturally, the higher the number of components, the better the match with experimental data; however, obtaining the analytical solution to the problem becomes more challenging.

In this study, we consider three Morse components (i = 0, 1, 2) to investigate neutron-proton (n-p) scattering encompassing all interactions between the nucleons, given as

$$U_0^{\rm RPA}(r) = V_0 + D_0[{\rm e}^{-2\alpha_0(r-r_0)} - 2{\rm e}^{-\alpha_0(r-r_0)}], \qquad r_0 < x_1, \quad (15)$$

$$U_1^{\rm RPA}(r) = V_1 + D_1[{\rm e}^{-2\alpha_1(r-r_1)} - 2{\rm e}^{-\alpha_1(r-r_1)}], \qquad x_1 < r_1 < x_2, \quad (16)$$

$$U_2^{\rm RPA}(r) = V_2 + D_2[{\rm e}^{-2\alpha_2(r-r_2)} - 2{\rm e}^{-\alpha_2(r-r_2)}], \qquad r_2 > x_2, \quad (17)$$

where x_1 and x_2 are two internal points that demarcate the three potentials, called as boundary points. These are also varied so that a large number of smooth curves would be available from the sample space to determine the most optimal solution. For ensuring smoothness of potential at the boundary points x_1 and x_2, between the three, the functions $U_0(r)|_{r=x_1} = U_1(r)|_{r=x_1}$ and $U_1(r)|_{r=x_2} = U_1(r)|_{r=x_2}$ and their derivatives must be continuous at x_1 and x_2. That is,

$$\frac{{\rm d}U_0(r)}{{\rm d}r}\Big|_{r=x_1} = \frac{{\rm d}U_1(r)}{{\rm d}r}\Big|_{r=x_1}, \quad (18)$$

$$\frac{{\rm d}U_1(r)}{{\rm d}r}\Big|_{r=x_2} = \frac{{\rm d}U_2(r)}{{\rm d}r}\Big|_{r=x_2}, \quad (19)$$

Using these equations, four of the twelve parameters are determined as

$$D_1 = \frac{\alpha_0 D_0 g_0}{\alpha_1 g_1}, \quad (20)$$

$$D_2 = \frac{\alpha_1 D_1 l_1}{\alpha_2 l_2}, \quad (21)$$

$$V_1 = V_2 + D_2 k_2 - D_1 k_1, \quad (22)$$

$$V_0 = V_1 + D_1 f_1 - D_0 f_0, \quad (23)$$

where the factors $f_0, f_1, g_0, g_1, k_1, k_2, l_1, l_2$ are given by

$$f_0 = {\rm e}^{-2\alpha_0(x_1-r_0)} - 2{\rm e}^{-\alpha_0(x_1-r_0)}$$
$$f_1 = {\rm e}^{-2\alpha_1(x_1-r_1)} - 2{\rm e}^{-\alpha_1(x_1-r_1)}, \quad (24)$$

$$g_0 = {\rm e}^{-2\alpha_0(x_1-r_0)} - {\rm e}^{-\alpha_0(x_1-r_0)}$$
$$g_1 = {\rm e}^{-2\alpha_1(x_1-r_1)} - {\rm e}^{-\alpha_1(x_1-r_1)}, \quad (25)$$

$$k_1 = {\rm e}^{-2\alpha_1(x_2-r_1)} - 2{\rm e}^{-\alpha_1(x_2-r_1)}$$
$$k_2 = {\rm e}^{-2\alpha_2(x_2-r_2)} - 2{\rm e}^{-\alpha_2(x_2-r_2)}, \quad (26)$$

$$l_1 = {\rm e}^{-2\alpha_1(x_2-r_1)} - {\rm e}^{-\alpha_1(x_2-r_1)}$$
$$l_2 = {\rm e}^{-2\alpha_2(x_2-r_2)} - {\rm e}^{-\alpha_2(x_2-r_2)}, \quad (27)$$

Therefore, we should optimize eight model parameters of three smoothly joined Morse functions, *i.e.*, α_0, α_1, α_2, r_0, r_1, r_2, V_2, and D_0. We also optimize the points x_1 and x_2 where the considered Morse functions are joined. Overall, we need to optimize 10 parameters to construct inverse scattering potentials for single channel scattering.

For many channel scattering, we need to construct three potentials by solving three coupled non-linear first-order equations simultaneously. For this, we need to optimize 30 parameters to obtain potentials corresponding to different total angular momenta, J, along with the tensor potential.

Hence, we optimize these required parameters by utilizing a physics-informed machine learning paradigm through the variable phase approximation, which is the inverse scattering method.

C. Machine learning (ML) based optimization

Manual optimization of parameters is a time-consuming and resource-intensive task, requiring experimentation with various combinations and settings. For expediting this process, optimization algorithms [29] are employed to efficiently determine the best configuration of model parameters. These algorithms iterate through numerous combinations to identify the optimal model configuration, surpassing the capabilities of human optimization.

In machine learning optimization, a loss function serves as a metric for assessing the disparity between actual and predicted output values. The objective is to reduce the error incurred by the loss function, thereby enhancing the model's accuracy in predicting outcomes.

There are various techniques that we may utilize to optimize a model. In this study, we employed a prominent optimization technique known as the GA [21, 30, 31]. The GA is an optimization method inspired by genetics and natural selection. It is commonly employed to discover optimal or close-to-optimal solutions for challenging problems that might otherwise be impractical to solve within a reasonable time-frame. Moreover, it is often used in research for solving optimization problems. While GAs do not necessarily involve explicit learning processes such as those found in supervised or reinforcement learning, they utilize principles inspired by biological evolution to iteratively improve candidate solutions to optimization problems. In GAs, a pool or population of potential solutions is subjected to recombination and mutation, similar to processes observed in natural genetics. This generates new offspring, and the cycle repeats across multiple generations. Each individual, representing a candidate solution, is evaluated based on its fitness, determined by the objective function value. Fitter individuals have a higher likelihood of reproducing, following the principle of "survival of the fittest" from Darwinian theory [21, 29].

Through successive generations, the algorithm evolves better solutions until a stopping criterion is met. While GAs involve randomness, they outperform simple random local search methods by leveraging historical information.

Process of GA The GA employs three primary sets of rules during each iteration to generate the succeeding generation from the current population [29]:

1. The selection process determines which individuals, referred to as parents, will be included in the population for the next generation. This selection is typically probabilistic and may consider the scores or fitness of the individuals.

2. Crossover rules merge two parents to create offspring for the subsequent generation.

3. The mutation rules introduce random alterations to individual parents, resulting in the formation of children.

Recombination and mutation are essential mechanisms in GAs for promoting exploration, maintaining genetic diversity, and preventing premature convergence. If their values are set too low, the optimization process may suffer from limited exploration, slow convergence, loss of diversity, and an increased risk of settling on suboptimal solutions. Therefore, it is crucial to carefully tune the values of recombination and mutation to achieve a balance between exploration and exploitation, leading to effective optimization outcomes.

The GA has many advantages over traditional optimization methods. Algorithms such as gradient descent and Newton's method rely on derivatives to find optimal solutions. They begin at a random point and iteratively move in the direction of the gradient until reaching a peak. While effective for problems such as linear regression with single-peaked objective functions, they struggle with real-world complexities featuring multiple peaks and valleys (non-convex objective functions). Traditional algorithms often get trapped at local optima in such scenarios [32]. In contrast, GAs bypass the need for objective function gradients. They are versatile, suitable for optimizing discontinuous, non-differentiable, stochastic, or highly non-linear functions. Moreover, GAs are easily parallelizable, fast, and capable of exploring vast search spaces efficiently. They can accommodate multiple complex optimization objectives.

Using this algorithm, we optimized the model parameters by minimizing the loss function called *MSE*, defined as

$$MSE = \frac{1}{N}\sum_{i=1}^{N}(\delta^{i}_{inp}(kr) - \delta^{i}_{\rm obt}(kr))^2, \tag{28}$$

In the inverse problem, the asymptotic phase shift values ($\delta(r\to\infty)$ at different energies are used as input to describe the unknown potential $V(r)$. Thus, ($\delta^{i}_{inp}(kr)$ are the input phase shifts that we took from the Granada database [33] at different energies for different ℓ channels. With these inputs, we optimized the model parameters of the reference potential using the GA and obtained phase shifts $\delta^{i}_{\rm obt}(kr)$ by solving phase equations. Using the optimized parameters, we constructed the inverse potentials $V(r)$.

III. RESULTS AND DISCUSSION

The scattering phase shift data for an np system comprises two S-states ($^3S_1$, $^1S_0$), 4 P-states ($^1P_1$), ($^3P_0$, $^3P_1$, $^3P_2$), 4 D-states ($^1D_2$), ($^3D_1$, $^3D_2$, $^3D_3$), 4 F-states ($^1F_3$), ($^3F_2$,$^3F_3$,$^3F_4$), 3 G-states ($^1G_4$), ($^3G_3$, $^3G_4$), and 1 H-state ($^3H_4$), i.e., a total of 18 states. Of these, eight of them have mixing due to the tensor potential, which results in four multi-channel states, ($^3S_1$, $^3D_1$), ($^3P_2$, $^3F_2$), ($^3D_3$, $^3G_3$), and ($^3F_4$, $^3H_4$). The Granada group considered a total of 6713 *np* and *pp* scattering data collected between 1950 and 2013 with a 3σ-self-consistent database, the largest collection of *NN* scattering for energies up to 350 MeV to date. They carefully considered all statistical versus systematic errors and refined the database to comprise only 11 data points at energies of 1, 5, 10, 25, 50, 100, 150, 200, 250, 300, and 350 MeV for each of these states and mixing parameters [33].

A. Optimization of potentials for single channel scattering

To construct inverse potentials for channels exhibiting single-channel scattering, we employ a 10-D parameter space. Optimization of these inverse potentials is

achieved through a GA, where the selection of bounds plays a pivotal role. For instance, let us consider the case of the $^1S_0$ state, necessitating the optimization of 10 parameters. For this, we generate a parameter space by specifying the bounds. Initially, we set the bounds as follows: $[\alpha_0, \alpha_1, \alpha_2, r_0, r_1, r_2, V_2, x_1, x_2, D_0]$ = [(0.01, 10), (0.01, 10), (0.01, 10), (0.01, 6), (0.01, 10), (0.01, 10), (0.01, 5), (0.01, 1), (1.01, 4), (0.01, 500)]. This creates a vast sample space for each parameter and constructs a family of curves, necessitating considerable time for convergence towards the optimal solution. Upon careful examination of the obtained optimized parameters after a few thousand iterations, we reduce the sample space for the parameters as [[(0.01, 2), (0.01, 10), (0.01, 2), (0.01, 6), (0.01, 2), (0.01, 5), (0, 0.01), (0.01, 1), (1, 4), (0.01, 100)]] to decrease computational time. The obtained MSE for the best solution, representing the interactions comprehensively, is on the order of 10^{-3}. The optimized model parameters for channels exhibiting single ℓ scattering are presented in Table 1.

During optimization, it was observed that the value of parameter V_2 approaches zero or is on the order of 10^{-8}. Hence, we omitted the value of V_2 in the table as it consistently tends towards zero for all channels. The MSE for the states having single channel scattering is also less than 10^{-3}. There is an advantage in utilizing three piecewise Morse functions as a reference as they offer three shape parameters, α_0, α_1, and α_2, in contrast to a single Morse function, which offers only one shape parameter, α_0. These shape parameters aid in elucidating the long-range part of the *NN* interaction without compromising the deep attractive nature expected for the intermediate region. This long-range part is often fitted by OPEP by many researchers [7]; however, in this study, we fit it phenomenologically using piece-wise Morse functions as a reference.

Using these optimized parameters, we construct inverse potentials and determine the corresponding scattering phase shifts by solving the phase equation, as depicted in Fig. 1 and Fig. 2. From these figures, the following observations are made:

1. For the $^1S_0$ state, the depth of the potential V_d is determined to be 97.87 MeV at a distance r_d of 0.84 fm. Observing the phase shifts depicted in Fig. 1, it is noted that they exhibit a decreasing trend, with positive values from an energy of 1 MeV up to 250 MeV. However, from 300 to 350 MeV, the phase shifts have negative values. This indicates that the constructed inverse potential must manifest an attractive nature for energies up to 250 MeV and a strong repulsive nature at short inter-nuclear distances that can be reached at very high energies. This is observed in Fig. 1(a).

2. For $\ell = 1$, there are three states: $^1P_1$, $^3P_0$, and $^3P_1$, each exhibiting single-channel scattering. In the case of the $^1P_1$ and $^3P_1$ states, it is observed that their phase shifts cross over after 200 MeV. Similarly, their respective inverse potentials cross over at approximately 1.48 fm. For $^3P_0$, phase shifts are initially positive and then cross over to negative values; the repulsive nature of the potential curve can be observed. The depth of potential V_d is 14.06 MeV at a distance r_d equal to 1.73 fm, as shown in Fig. 1(b).

3. For $\ell = 2$, there are two single channel states, namely $^1D_2$ and $^3D_2$. For the state $^1D_2$, the phase shifts are consistently positive, indicating an attractive nature. The obtained inverse potentials are purely attractive, with a depth V_d of 109.76 MeV observed at a distance r_d of 0.99 fm. Conversely, for the state $^3D_2$, the phase shift values exhibit an increasing trend from 1 MeV to 300 MeV. However, at 350 MeV, the phase shift value decreases, indicating a transition from increasing to decreasing behavior. Consequently, the constructed inverse potentials exhibit both repulsive and attractive characteristics. The depth of potential V_d is determined to be 52.96 MeV at a distance r_d of 0.25 fm, as shown in Fig. 2(c).

4. For $\ell = 3$, $^1F_3$ and $^3F_3$ are single-channel scatter-

Table 1. Optimized model parameters for channels exhibiting single-channel scattering.

States	α_0	α_1	α_2	r_0	r_1	r_2	x_1	x_2	D_0
$^1S_0$	1.9279	3.2968	1.2739	1.5652	0.8408	0.6625	0.1447	2.5943	65.548
$^1P_1$	0.5291	1.226	0.902	2.892	2.725	0.1209	0.3838	2.412	86.5373
$^3P_0$	0.4833	2.1083	1.107	3.6406	1.7308	1.739	1.3573	3.7105	25.8011
$^3P_1$	0.4038	0.3509	1.066	3.2984	1.9282	1.1887	0.0862	1.9142	99.8203
$^1D_2$	1.6731	2.1799	1.1822	0.1951	0.4325	0.6853	0.5247	3.2577	62.9885
$^3D_2$	0.4772	1.6048	0.9652	3.9727	0.9912	0.01	0.4254	4.1974	26.8804
$^1F_3$	0.2786	2.1457	0.9051	4.6928	0.2598	0.3213	0.5347	3.0394	33.2355
$^3F_3$	1.5956	3.9514	0.9899	0.6209	1.9159	1.6301	1.8396	3.0465	76.5406
$^1G_4$	0.1592	2.1651	1.0086	6.5931	0.666	1.433	0.5038	3.2474	31.7747
$^3G_4$	0.2439	1.4924	0.9587	2.0183	0.5926	0.1479	0.4721	3.9713	83.3077

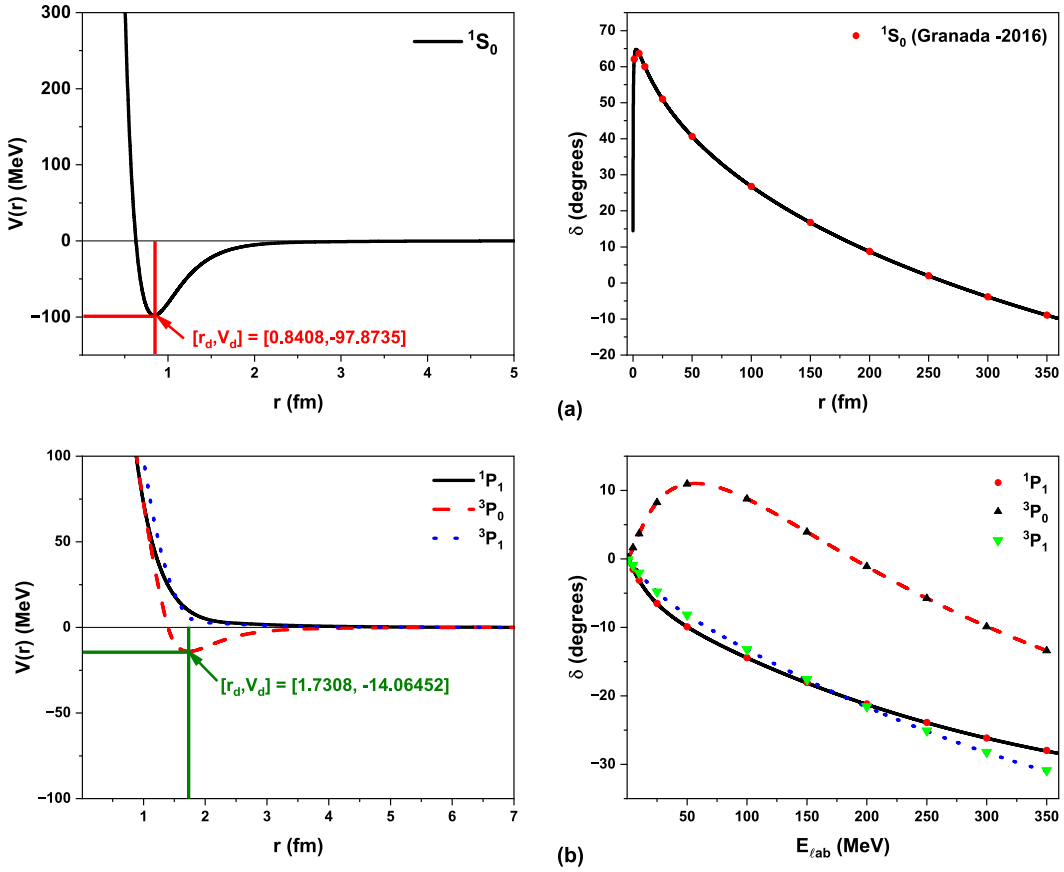

Fig. 1. (color online) Inverse potentials along with scattering phase shifts for single channel scattering for S and P waves.

ing states. For $^1F_3$, the phase shifts are consistently negative, indicating an increase in repulsion as the inter-nucleon distance decreases. For $^3F_3$, the phase shifts exhibit a negative trend, initially increasing from 1 MeV to 300 MeV, after which they decrease. This trend resembles a negative parabola. As a result, the obtained inverse potentials encompass both repulsive and attractive components. However, beyond a distance of 1.62 fm, the nature of the potential shifts predominantly towards repulsion, mirroring the change in the nature of the phase shifts. The depth of the obtained potential, denoted as V_d, is measured to be 42.86 MeV at a distance r_d equal to 0.62 fm, as illustrated in Fig. 2(d).

5. There are two states, namely $^1G_4$ and $^3G_4$, having single channel scattering for $\ell = 4$. For both states, the phase shifts are positive, and hence, the obtained inverse potentials are attractive. For $^1G_4$ and $^3G_4$, the depths V_d are 27.95 MeV and 38.75 MeV, observed at distances r_d of 0.28 fm and 0.62 fm, respectively, as depicted in Fig. 2(d).

B. Optimization of potentials for multi-channel scattering

In the np system, there exist four channels where coupling is observed. The degree of this coupling is delineated by the mixing parameters, denoted by ϵ, which elucidate the interaction between two states within a specific channel. For many channel scattering, we incorporated the mixing parameter using "Stapp Parametrization" [10] and solved the three coupled non-linear differential equations. From these equations, we optimized 30 parameters and constructed three inverse potentials corresponding to individual states and their mixing parameters. The potentials corresponding to the mixing parameter are the tensor potentials, which we obtained directly by solving the coupled equations. Constructing these three potentials simultaneously is a challenge as we have a 30 D parameter space. Adjusting the bounds of these parameters is a crucial task in the GA. To obtain the most optimal solutions, we adjusted the bounds by solving the single-channel phase equation and determined where the possible solutions of the equation occurs. Thus, after obtaining an approximate idea about the bounds, we readjusted them to solve the multi-channel scattering equations. To obtain the best possible potentials, we calculated the MSE of three equations individually and optimized the mean of these MSEs by adjusting their weights. Initially, the S, D, and mixing channels were given equal weightage in determining the mean of their MSE values. While the outputs of S and D channels closely matched,

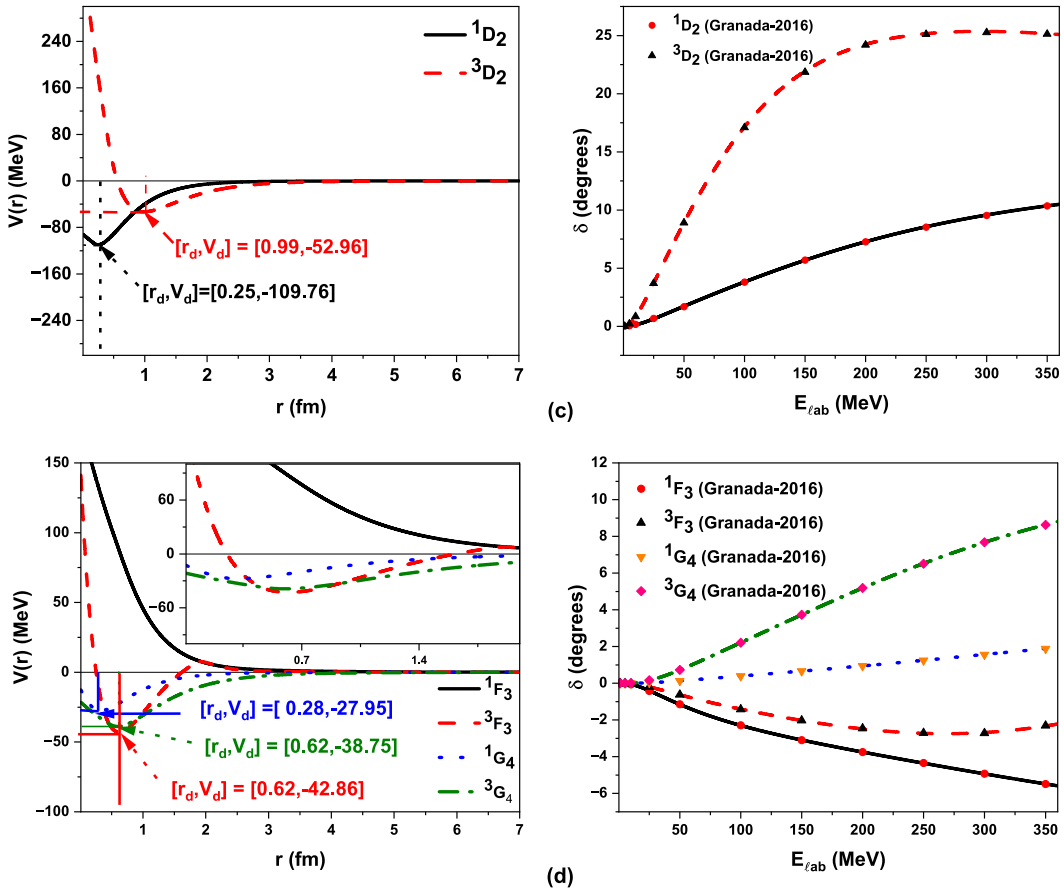

Fig. 2. (color online) Inverse potentials along with scattering phase shifts for single channel scattering for D, F, and G waves.

those of the mixing channel did not. This is because the phase shift values for S and D channels were significantly larger than those owing to their coupling. We observed that the relative error in phase shifts due to coupling were much higher than those due to individual channels without mixing. Hence, we doubled the weightage for the MSE obtained for mixing parameters in the formula for the mean of MSEs, which improved the results. The optimized model parameters for multi-channel scattering are given in Table 2. The obtained MSEs for these channels are on the order of 10^{-2}. The constructed inverse potentials along with their corresponding phase shifts are depicted in Fig. 3 and Fig. 4. The following observations are made:

1. For $J = 1$, coupling exists between $^3S_1$ and $^3D_1$ states. The constructed inverse potentials corresponding to these states are shown in Fig. 3(e). The phase shift values of the $^3S_1$ state are in decreasing order and hence exhibit both repulsive and attractive natures having a depth of 87.90 MeV at distance r_d to be 0.86 fm. The values of phase shifts of the $^3D_1$ state is negative, and hence, the potential is repulsive in nature. The values of mixing parameter ϵ_1 is negative, and hence, the potential is attractive in nature having depth of 309.97 MeV at distance r_d to be 0.40 fm.

2. For $J = 2$, coupling exists between $^3P_2$ and $^3F_2$ states. The potentials of $^3P_2$ and $^3F_2$ are both repulsive and attractive, with depths V_d equal to 72.75 MeV and 3.34 MeV at distances r_d of 0.24 fm and 2.24 fm, respectively, as depicted in Fig. 3(f). The values of mixing parameter ϵ_2 are negative, and hence, the nature of the tensor potential is repulsive.

3. For $J = 3$, coupling exists between $^3D_3$ and $^3G_3$ states. Both $^3D_3$ and $^3G_3$ states have a repulsive potential. Regarding the mixing parameter ϵ_3, the constructed inverse potential is attractive in nature, as depicted in Fig. 4(g).

4. For $J = 4$, coupling exists between $^3F_4$ and $^3H_4$ states. In the $^3F_4$ state, the phase shift values increase positively, resulting in an inverse potential exhibiting both repulsive and attractive characteristics, with a depth V_d of 13.71 MeV at a distance r_d of 1.41 fm. Conversely, for the $^3H_4$ state, the phase shifts are positive, indicating an attractive nature of the potential, with a depth V_d of 14.99 MeV at a distance r_d of 0.64 fm, as illustrated in Fig. 4(h). The mixing parameter ϵ_4 takes negative values in increasing order, implying attraction up to 0.64 fm, beyond which repulsion emerges. Consequently, the tensor potential exhibits a more repulsive nature corresponding to ϵ_4, as clearly depicted in Fig. 4(h).

Table 2. Optimized model parameters for channels exhibiting many-channel scattering.

States	α_0	α_1	α_2	r_0	r_1	r_2	x_1	x_2	D_0
$^3S_1$	1.7864	3.5192	1.2176	2.2299	0.8673	7.9764	0.0218	1.6569	23.0292
ϵ_1	1.0242	2.5235	1.3197	2.0600	0.4000	0.0100	0.0100	2.3578	57.7110
$^3D_1$	0.3691	1.6372	1.0521	3.4736	0.0108	0.0119	0.3218	3.6187	29.1949
$^3P_2$	1.0257	3.1263	1.1437	2.6544	0.5451	4.9708	0.0100	1.4440	23.3281
ϵ_2	1.7441	0.3447	0.7514	0.0103	0.4897	14.2702	0.4074	0.5890	93.5844
$^3F_2$	0.6345	0.6979	2.0917	1.6293	0.1262	2.2408	0.5927	1.9031	12.2068
$^3D_3$	0.5912	1.5485	1.6835	1.9402	2.3206	3.0536	0.0956	1.9256	72.7436
ϵ_3	0.3993	1.6200	1.0660	1.4897	0.0424	0.0129	0.0141	3.6925	32.5026
$^3G_3$	0.1773	1.5757	1.3185	5.2381	0.5666	1.0581	0.7447	2.6793	19.4466
$^3F_4$	0.9507	2.8765	0.6763	2.1921	1.4048	8.2111	0.8588	3.7172	75.5033
ϵ_4	0.6376	1.4582	0.5219	0.0123	1.3187	16.1720	1.0822	4.7992	50.7831
$^3H_4$	0.5228	1.2174	1.8201	0.7222	0.6374	0.2356	0.3636	2.1788	86.7397

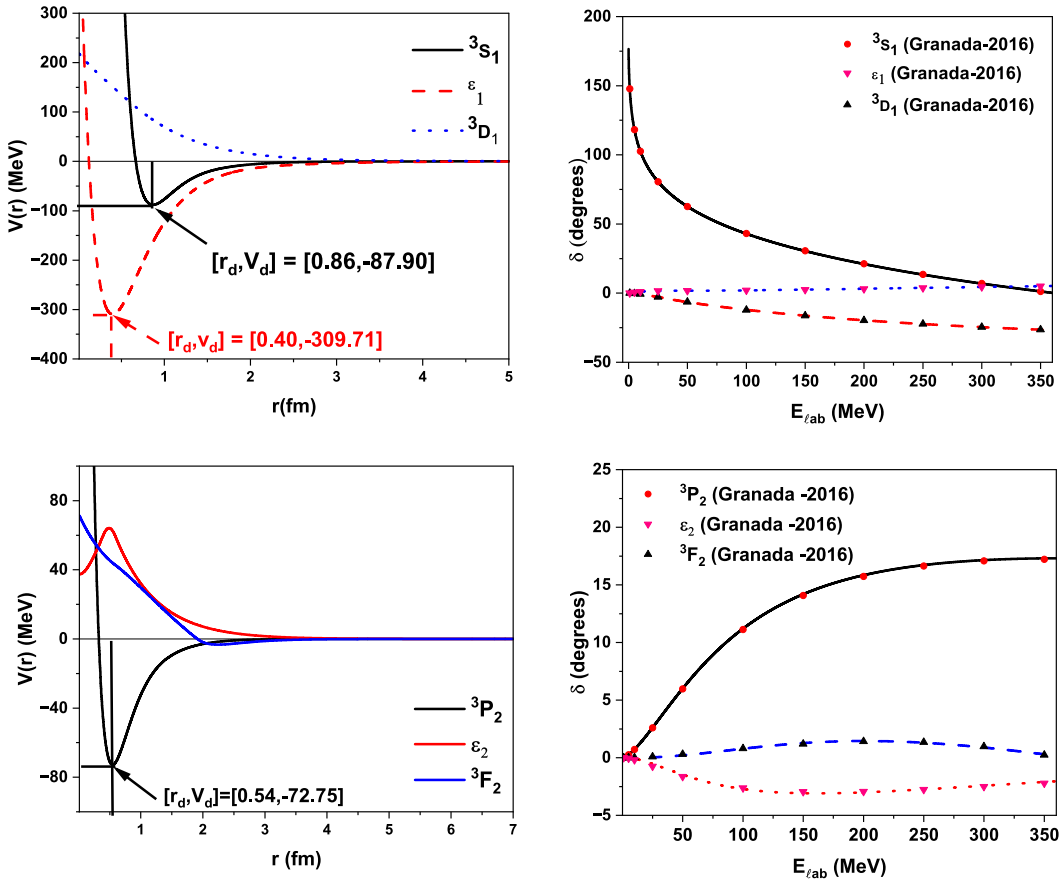

Fig. 3. (color online) Inverse potentials along with scattering phase shifts for the multi channel scattering of $J = 1$ and 2.

C. Low energy scattering parameters

Using the obtained scattering phase shifts, we can calculate the low energy scattering parameters for the S state by utilizing the effective range approximation formula [34], which is given as

$$k\cot\delta_0 = -\frac{1}{a_0} + \frac{1}{2}rk^2 + \ldots, \tag{29}$$

where k is the centre of mass momentum, δ_0 is the phase shift for $\ell = 0$, a_0 is the scattering length, and r is the effective range. Using the obtained phase shifts, we calcu-

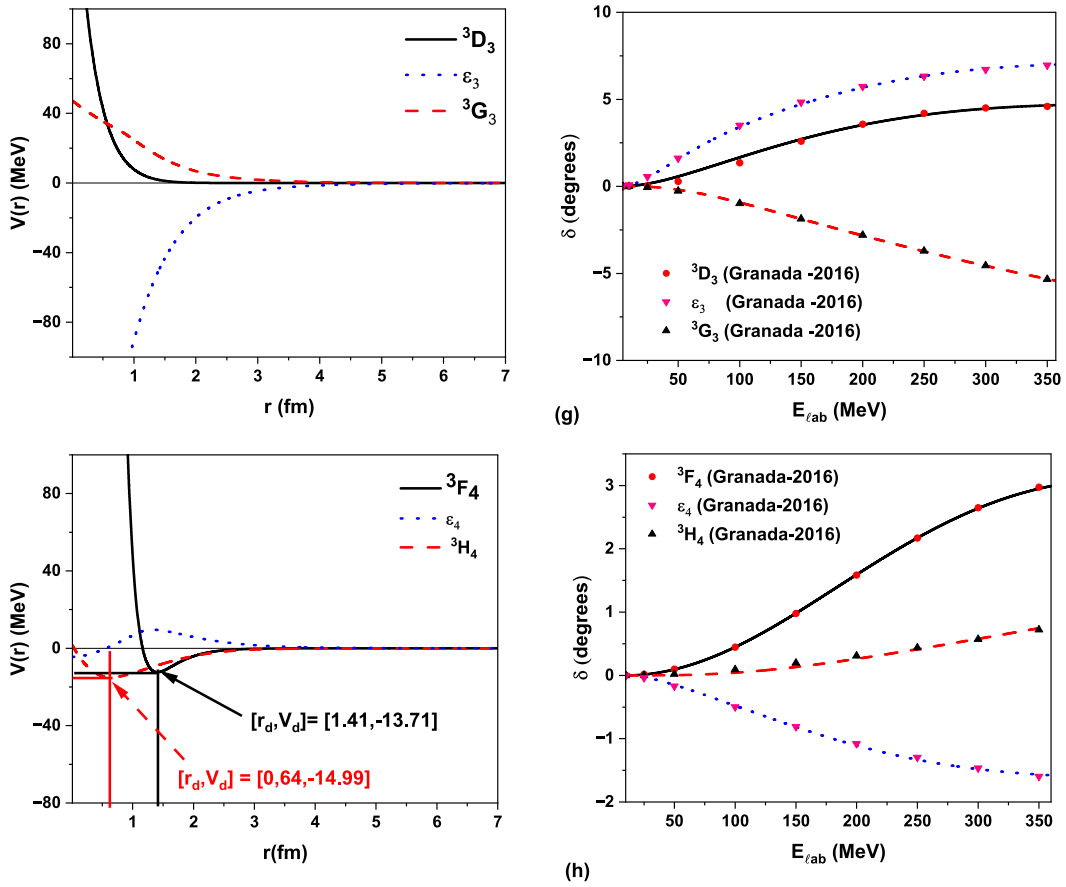

Fig. 4. (color online) Inverse potentials along with scattering phase shifts for the multi channel scattering of $J = 3$ and 4.

late the low energy scattering parameters as given in Table 3. In Table 3, we compare our results with the most successful high precision potential such as the Av_{18} potential [1] and Granada-2016 [31]. The scattering parameters obtained for the $^3S_1$ state exhibit a remarkable alignment with experimental values, demonstrating a precise match with an error margin of less than 0.6%. For $^1S_0$, the scattering length matches well with the experiment within an error of 0.03%; however, for the effective range, there is some discrepancy between our calculations and the experimental results. This may be owing to any possible error in input phase shifts of $^1S_0$. The effective range for $^1S_0$ given by the Av_{18} potential and Granada-2016 are 2.69 fm and 2.67 fm , respectively.

D. Partial and total cross-sections

Utilizing the obtained phase shifts, we calculate the partial cross-section $\sigma_\ell(E)$ [16, 36] for *n-p* scattering as

$$\sigma_\ell(E;S,J) = \frac{4\pi}{k^2}\sum_{S=0}^{1}\left(\sum_{J=|\ell-S|}^{|\ell+S|}(2\ell+1)\sin^2(\delta_\ell(E;S,J))\right), \quad (30)$$

and thus, the total scattering cross section (SCS), σ_T, [16] is given as

$$\sigma_T(E;S,J) = \frac{1}{\sum_{J=|\ell-S|}^{|\ell+S|}(2J+1)}\sum_{\ell=0}^{n}\sum_{S=0}^{1}(2J+1)\sigma_\ell(E;S,J), \quad (31)$$

Here, "n" is the number of ℓ- channel data points available for the scattering system. In our study, we take $n = 5$ for all five ℓ channels. The total scattering cross section closely matches the experimental ones [37], as depicted in Fig. 5, within an experimental error of less than 1%. The inset of Fig. 5 represents the contribution of both $^1S_0$ and $^3S_1$ states in the total cross section. One can observe that the contribution of $^1S_0$ is large at low energies below 1 MeV, gradually decreases with increasing energy, and becomes considerably small beyond 100 MeV. In contrast, the contribution from the $^3S_1$ state increases beyond 1 MeV , peaks at 10 MeV , and then decreases. One can also observe that, as energy levels increases from 100 MeV to 350 MeV, the contributions from *P* and *D* channels become notably significant, whereas those from *F* and *G* states remain comparatively less pronounced within the same range. However, they become increasingly important for accurately representing the observed experimental total SCS. Contributions from the 1 *H*-state are minimal and have negligible impact on de-

Table 3. Low energy scattering parameters of $^1S_0$ and $^3S_1$ states. We compare our calculations with realistic potentials such as Av-18 [1] and Granada-2016 [33].

States	Scattering length 'a_0' /fm				Effective range "r" /fm			
	Exp [35]	Av_{18} [1]	Granada 2016 [33]	**Our work**	Exp [35]	Av_{18} [1]	Granada 2016 [33]	**Our work**
$^1S_0$	–23.749(8)	–23.732	–23.735	**–23.741**	2.81(5)	2.697	2.673	**2.63**
$^3S_1$	5.424(3)	5.419	5.441	**5.445**	1.760(5)	1.75	1.781	**1.770**

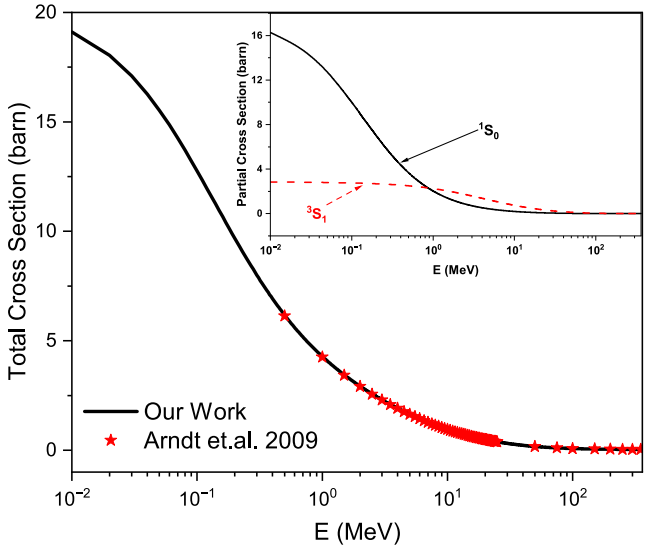

Fig. 5. (color online) Obtained total scattering cross section (SCS) along with the experimental SCS [37]. The energy is plotted on a log scale. The inset shows contributions due to both $^1S_0$ and $^3S_1$ states.

termining the total SCS. Hence, the obtained total scattering cross sections closely align with experimental observations [37]. The computed partial and total cross-section values at various energies, alongside experimental values, are compiled in Table 4.

IV. CONCLUSIONS

The approach of inverse scattering theory realized computationally through the reference potential approach is equivalent to the physics informed machine learning paradigm. Instead of adjusting weights in a neural network to obtain the underlying optimization function that best describes the expected data [33], here, the parameters of a piece-wise smooth Morse function are varied utilizing the GA [21] to simulate all possible shapes of curves that span a sample space from which one converges to the best model potential. The resultant inverse potentials for various ℓ channels are phenomenological in the sense that they take into account all possible interactions within the scattering particles. Our potentials are in good agreement with existing high precision realistic potentials, based on modeling various internal interactions, thus validating our computational approach and paving the way for an alternative methodology to understand the inherent nature of interactions in various scattering scenarios. In particular, this reference potential approach leads to an elegant solution for charged particle scattering [38], where modeling the Coulomb interaction poses a major challenge. In conclusion, our computational methodology to construct inverse potentials based on piece-wise smooth Morse functions as a reference family of curves using the GA for optimization is successful in explaining

Table 4. Individual contributions of different channels to the overall calculated total elastic scattering cross-section (SCS). The percentage contributions of these channels to the total obtained SCS are indicated in parentheses.

E /MeV	$\sigma_{\rm exp}$ [37] (barn)	σ_S	σ_P	σ_D	σ_F	σ_G	σ_H	$\sigma_{\rm sim}$ (barn)
1	4.253	4.283 (100%)	0.000	0.000	0.000	0.000	0.000	4.283
5	1.635	1.635 (99.8%)	0.002 (0.2%)	0.000	0.000	0.000	0.000	1.638
10	0.9455	0.9399 (99.3%)	0.0059 (0.6%)	0.0004 (0.1%)	0.0000	0.0000	0.0000	0.9462
25	0.3804	0.3673 (96%)	0.0124 (3.2%)	0.0030 (0.8%)	0.0001	0.0000	0.0000	0.3828
50	0.1684	0.1455 (85.5%)	0.0159 (9.3%)	0.0085 (5%)	0.0002 (0.1%)	0.00000	0.00000	0.1701
100	0.07553	0.04162 (55.1%)	0.01761 (23.3%)	0.01547 (20.5%)	0.00053 (0.7%)	0.00025 (0.3%)	0.00000	0.07549
150	0.05224	0.0148 (28.7%)	0.01837 (35.5%)	0.01734 (33.5%)	0.00069 (1.3%)	0.00052 (1%)	0.00000	0.05175
200	0.04304	0.00534 (12.6%)	0.01883 (44.3%)	0.01678 (39.5%)	0.00073 (1.7%)	0.00079 (1.9%)	0.00000	0.04248
250	0.03835	0.00169 (4.5%)	0.01905 (50.2%)	0.01547 (40.8%)	0.00069 (1.8%)	0.00103 (2.7%)	0.00000	0.03794
300	0.03561	0.00042 (1.2%)	0.01902 (53.8%)	0.01404 (39.7%)	0.00064 (1.8%)	0.00122 (3.4%)	0.00001	0.03535
350	0.03411	0.00019 (0.6%)	0.01878 (55.7%)	0.01270 (37.7%)	0.00066 (2%)	0.00136 (4%)	0.00001	0.0337

the experimental outcomes of *np*-scattering. Our scattering parameters match closely with those obtained by Argonne and Granada researchers. The calculated total cross-sections from the simulated scattering phase shifts are highly similar to the experimental ones, thus validating our reference potential approach. The constructed potentials can be utilized to determine the off-shell properties of the deuteron, such as its binding energy and structural electromagnetic form factors. These aspects will be addressed separately. Moreover, these inverse potentials for various neutron-proton scattering states would be useful in nuclear ab-initio calculations.

ACKNOWLEDGEMENTS

We would like to acknowledge the contributions of Mr. M. G. Ganesh Kumar, who enhanced the efficiency of the code, and Dr. Anil Khachi, for his preliminary discussions on mixing parameters.

DATA AVAILABILITY

The datasets that were used and/or analyzed during this study are available from the Granada Database. https://www.ugr.es/~amaro/nndatabase/database.php/

References

[1] R. B. Wiringa, V. G. J. Stoks and R. Schiavilla, Phys. Rev. C. **51**, 38 (1995)
[2] R. Machleidt, Phys. Rev. C **63**, 024001 (2001)
[3] R.V. Reid, Annals of Physics **50**, 411 (1968)
[4] V. G. J. Stoks, R. A. M. Klomp, C. P. F. Terheggen *et al*., Phys. Rev. C. **49**, 2950 (1994)
[5] M. Lacombe, B. Loiseau, J. M. Richard *et al*., Phys. Rev. C **21**, 861 (1980)
[6] T. Ericson and W. Weise, *Pions and Nuclei* (Clarendon Press, Oxford, 1988)
[7] M. Naghdi, Phys. Part. Nuc. **45**, 924 (2014)
[8] P. M. Morse and W. P. Allis, Phys. Rev. **44**(4), 269 (1933)
[9] F. Calogero, *Variable Phase Approach to Potential Scattering*, First edition (Elsevier, 1967)
[10] V. Babiko, Soviet Physics Uspekhi **10**(3), 271 (1967)
[11] G. Balassa, Eur. Phys. J. A **58**(9), 186 (2022)
[12] M. Selg, Mol. Phys. **104**, 2671 (2006)
[13] M. Karimi-Mamaghan, M. Mohammadi, P. Meyer *et al*., Eur. J. Oper. Res. **296**(2), 393 (2022)
[14] G. E. Karniadakis, I. G. Kevrekidis, L. Lu *et al*., Nat. Rev. Phys. **3**(6), 422 (2021)
[15] M. Selg, Proc. Est. Academy Sciences **65**(3), 267 (2016)
[16] A. Khachi, L. Kumar, A. Awasthi *et al*., Physica Scripta **98**, 095301 (2023)
[17] A. Khachi, L. Kumar, M. R. Ganesh *et al*., Phys. Rev. C. **107**(6), 064002 (2023)
[18] O. S. K. S. Sastri, A. Khachi, and L. Kumar, Braz. J. Phys. **52**(2), 58 (2022)
[19] S. Deb, Resonance **19**, 713 (2014)
[20] M. Selg, J. Chem. Phys. **136**(11), 114113 (2012)
[21] S. Katoch, S. S. Chauhan, and V. Kumar, Multimed Tools Appl. **80**, 8091 (2021)
[22] H. S. Hans, *Nuclear Physics: experimental and theoretical*, (New Age International (P) Ltd. Publishers 2008), p. 100
[23] G. Balassa, Prog. of Theor. and Exper. Phys. **2023**(11), 113A01 (2023)
[24] V. I. Zhaba, Mod. Phys. Lett. A **31**(08), 1650049 (2016)
[25] G. J. Kynch, Proc. Phys. Soc. A **65**(2), 83 (1952)
[26] V. V. Babikov, *Some Methods of Calculating the Potential Scattering Parameters*, (Joint Institute for Nuclear Research, Dubna, USSR Laboratory of Nuclear Reactions 1964)
[27] J. R. Cox and A. Perlmutter, Il Nuovo Cimento **37**, 76 (1954)
[28] V. I. Zhaba, World Sci. News **129**, 255 (2019)
[29] X. S. Yang, in *Computational Optimization, Methods and Algorithms*, Vol. 356, edited by S. Koziel, X. S. Yang (Springer Berlin Heidelberg, 1970), p. 13-31
[30] K. F. Man, K. S. Tang, and S. Kwong, IEEE transactions on Industrial Electronics **43**(5), 519 (1996)
[31] M. John, J. Comp. App. Math. **184**(1), 205 (2005)
[32] P. Rebentrost, S. Maria, W. Leonard *et al*., New J. Phys. **21**(7), 073023 (2019)
[33] R. N. Pérez, J. E. Amaro, and E. R. Arriola, J. Phys. G: Nucl. and Part. Phys. **43**(11), 114001 (2016)
[34] V. A. Babenko and N. M. Petrov, arXiv: 1605.04849
[35] L. Koester and W. Nistler, Zeitschrift für Physik A Atoms and Nuclei **272**, 189 (1975)
[36] C. Amsler, *Nuclear and particle physics*, (IOP Publishing 2015)
[37] R. A. Arndt, W. J. Briscoe, and A. B. Laptev, Nucl. Sci. Eng. **162**, 312 (2009)
[38] O. S. K. S. Sastri, A. Sharma, and A. Awasthi, Phys. Rev. C **109**, 064004 (2024)